Single grain infrared photoluminescence (IRPL) measurements of feldspars for dating

Duller, G. A.T.; Gunn, Matt; Roberts, H. M.

Published in:
Radiation Measurements

DOI:
10.1016/j.radmeas.2020.106313

Publication date:
2020

Citation for published version (APA):
Duller, G. A. T., Gunn, M., & Roberts, H. M. (2020). Single grain infrared photoluminescence (IRPL) measurements of feldspars for dating. *Radiation Measurements*, *133*, [106313]. https://doi.org/10.1016/j.radmeas.2020.106313

Radiation Measurements 133 (2020) 106313

Contents lists available at ScienceDirect

Radiation Measurements

journal homepage: http://www.elsevier.com/locate/radmeas

Single grain infrared photoluminescence (IRPL) measurements of feldspars for dating

G.A.T. Duller [a,*], M. Gunn [b], H.M. Roberts [a]

[a] Department of Geography and Earth Sciences, Aberystwyth University, UK
[b] Department of Physics, Aberystwyth University, UK

ARTICLE INFO

Keywords:
Luminescence
Imaging
EM-CCD
Feldspar
Dose determination

ABSTRACT

Existing infrared photoluminescence (IRPL) systems have used pulsed infrared stimulation (~830 nm) and measured IRPL emission (at 880 or 955 nm) using time resolved data collection with photomultipliers. Breakthrough of the infrared stimulation light overwhelms the IRPL, but the delayed emission during the laser-off period has been used instead.

This paper describes a system for measurement of the IRPL signal from single sand-sized grains of feldspar. The attachment uses an electron-multiplying charge-coupled device (EMCCD) imaging system, and has two innovations that make it possible to use such a detector to obtain IRPL data. First, the optical detection system has been designed to minimise stray light and maximise the efficiency with which filters reject the stimulation light. This acts to reduce, but not eliminate, the breakthrough. Second, by placing the sample to be measured in a clearly defined sample grid, the spatial resolution provided by the EMCCD has been used to differentiate between regions of the image where IRPL is emitted and adjacent regions where only breakthrough is expected. This allows quantification of the breakthrough and effective subtraction to isolate the IRPL signal from the grains of interest.

The attachment has been used to measure IRPL from single sand-sized grains of feldspar from an aeolian dune from New Zealand. A 1W UV LED (365 nm) is also added to the system and this is effective at resetting the IRPL signal, permitting a single aliquot regenerative dose (SAR) protocol to be used to measure equivalent dose (D_e). Measurement of a known laboratory dose (104 Gy) demonstrates the reproducibility of the attachment, with no overdispersion observed in the resulting single grain D_e values. The recovered dose is within 10% of the given dose. The natural IRPL signal yields D_e values from single grains with low overdispersion (22%) and giving a weighted mean value (103 ± 5.8 Gy) that is consistent with that obtained using post-IR IRSL measurements (105 ± 3.8 Gy). The attachment described here provides IRPL measurements on single grains suitable for exploring the potential of this novel and exciting signal for dating geological sediments.

1. Introduction

The discovery of a luminescence emission at 955 nm in feldspars when stimulated in the near infrared (Prasad et al., 2017) opens up exciting new opportunities for archaeological and geological dating applications. This infrared photoluminescence signal (IRPL) signal, and a second emission at 880 nm (Kumar et al., 2018), are reported to have a number of properties that make them attractive for dating. First, the signal does not deplete during measurement, making it possible to improve the precision of individual measurements by extending the period of stimulation. Secondly, the signal is thought not to suffer from anomalous fading, a major challenge for other methods based on analysis of stimulated luminescence from feldspars. However, an additional observation in initial measurements (Prasad et al., 2017) is that the signal does not bleach rapidly with exposure to daylight, and this could potentially be an impediment to the use of this signal for dating sediments. In previous research using other luminescence signals, where the exposure of sediments to daylight may vary from one mineral grain to another, single grain measurements have proven valuable for dating (Duller, 2008). This paper describes the development of instrumentation for measuring the 955 nm IRPL emission from single sand-sized (~200 μm diameter) feldspar grains. The performance of this instrumentation

* Corresponding author.
E-mail address: ggd@aber.ac.uk (G.A.T. Duller).

https://doi.org/10.1016/j.radmeas.2020.106313
Received 26 August 2019; Received in revised form 12 January 2020; Accepted 12 March 2020
Available online 19 March 2020
1350-4487/

is assessed using potassium-rich feldspar from a sample of aeolian sand from New Zealand.

Kook et al. (2018) describe three approaches for measuring IRPL using an 830 nm laser for stimulation, and then a combination of long pass filters at 925 nm (LP925) and a band pass filter at 950 nm (BP950) to reject the stimulation light, and allow transmission of IRPL at 880 or 955 nm. Although the LP925 and BP950 filters have very low transmission at 830 nm when light strikes them normally, their performance is degraded significantly when light passes through obliquely (Fig. 1(a) and (b)), and breakthrough of the 830 nm stimulation light into the detector is a major problem. Two of the three systems that Kook et al. (2018) describe pulse the 830 nm IR laser (typically 5 μs on pulse, 95 μs off period) and use time resolved measurements with IR sensitive photomultiplier tubes so that they can ignore the signal during the on-period of the 830 nm stimulation and just use the IRPL emission in the off-period of the 830 nm laser (typically the period 3–92μs after each IR pulse). In order to make measurements of single grains of feldspar, they based one system around a focussed laser system (Duller et al., 2003). Kook et al. (2018) also describe a system based around use of an electron multiplying charge coupled device (EMCCD) camera. The EMCCD detector described by Kook et al. (2015) has been shown to be a sensitive detector capable of resolving luminescence emissions from single grains of quartz (Thomsen et al., 2015) at ~340 nm. However, unlike typical photomultipliers used for luminescence dating (e.g. ET EMD-9107 or EMI 9635) the EMCCD also has high sensitivity at wavelengths in the yellow (e.g. 580 nm, see Duller et al., 2015) and into the infrared, including up to 955 nm (Kook et al., 2018). Kook et al. (2018) showed an image of IRPL collected using the EMCCD, but no analytical data are shown, possibly because of the high breakthrough of the IR stimulation into the detector. Due to the reset and readout clock speeds, EMCCD images cannot be collected at a rate suitable for time-resolved measurements.

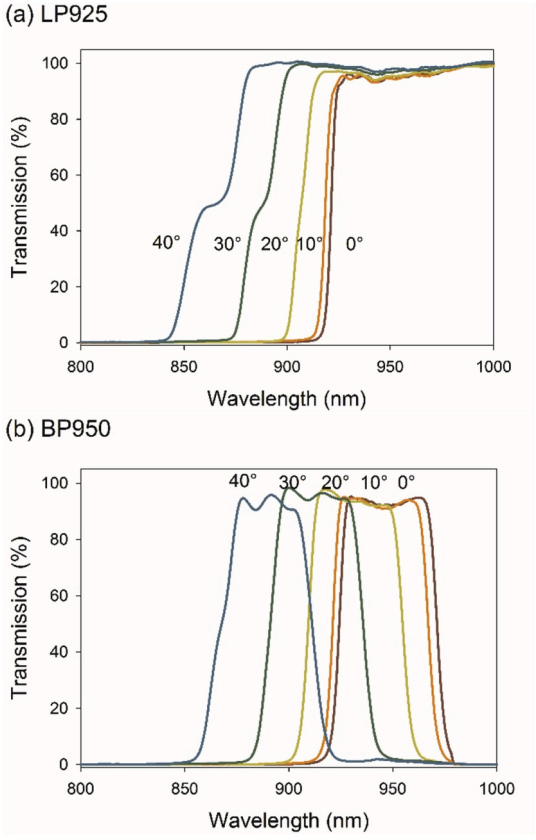

Fig. 1. (a) Transmission characteristics of LP925 when measured at angles from zero to 40° from perpendicular. (b) Similar data as shown in (a) but for the BP950 filter.

The aim of this work is to design an attachment for the Risø TL/OSL reader to measure IRPL from single mineral grains using an EMCCD. Two approaches are described that make this possible. Firstly, an optical design is described that optimises the performance of the detection filters in rejecting the stimulation light. Secondly, the spatially resolved nature of the data is exploited to provide an assessment of the breakthrough during every data collection, allowing this breakthrough signal to be effectively subtracted, yielding the IRPL signal. The performance of the attachment is demonstrated in a series of measurements of laboratory and natural doses.

2. Instrument description

Following the work of Kook et al. (2018) the Evolve EMCCD camera (Photometrics) was mounted on a Risø TL/OSL reader, but this was done using a bespoke head and detection optics designed and manufactured at Aberystwyth University to reduce the breakthrough of the IR stimulation (Fig. 2). The head has ports at 45°for optical stimulation of the sample using a 200 mW 850 nm IR laser diode mounted in a Thorlabs TEC temperature-controlled mount. The diode is driven from a Thorlabs bench top laser diode current controller operated in constant power mode with feedback provided by the laser diodes inbuilt photodiode. The laser diode output is cleaned up with an Edmund Optics BP850 × 10 nm OD4 filter to remove the low level but broad tails in its emission. The laser was scattered by a ground glass diffuser to provide uniform illumination with an irradiance of 20 mW cm^{-2} at the sample. On the detection side, the 850 nm stimulation was rejected using three Edmund Optics LP925 OD4 filters, and a BP950 x 50 OD4 filter was used to isolate the 955 nm emission (Fig. 1). This is the same filter combination described by Kook et al. (2018). The filters are interference filters designed to operate with light arriving perpendicular to the filter surface, and their transmission properties shift progressively to shorter wavelength as the angle of incidence of light on the filters increases (Fig. 1(a) and (b)). An examination of the Risø DASH head (see Fig. 2 in Lapp et al., 2015.) indicates that light can reach the filters at large angles of incidence with a small number of scattering events from the inside of the head and lens tube. The reflectance of the black anodise on the head was measured to be in excess of 20% at 850 nm, and so the likelihood of this happening is large. A critical part of the design of the IRPL head discussed in the present paper has been to control stray light to prevent the stimulation light reaching the filters at large angles of incidence. This has been achieved in two ways. Firstly, long focal length imaging optics along with a baffle located near the sample are used to restrict the angles of rays entering the optical system as shown in Fig. 2. The imaging optics consist of 100 mm and 80 mm Anti-Reflection coated IR achromatic doublets to achieve a magnification of 0.8 with the filters located between the lenses. Secondly, stray light has been minimised by coating all surfaces in the optical assembly with a matt black paint with a reflectance of less than 4% at 850 nm. The combination of these two approaches has meant that it has been possible to reduce the breakthrough to a level where IRPL can be measured using the EMCCD, and this is described in the remainder of this paper.

The head designed for IRPL measurements has eight ports where stimulation or detection units may be placed (Fig. 2) and one of these was fitted with a 300 mW 880 nm LED delivering ~40 mW cm^{-2} at the sample. Although an Electron Tubes EMD-9107 PMT was also mounted on the head, the collection efficiency was very poor due to the viewing geometry and limited aperture of the collecting optics, meaning that it was not possible to make IRSL measurements. Where IRSL measurements were needed, a DASH head Lapp et al (2015) equipped with 870 nm IR LEDs (180 mW cm^{-2}) was used, fitted with a BG3 and BG-39 filter.

Resetting the IRPL signal has been reported as difficult (Prasad et al., 2017) so we mounted a 1W 365 nm Thorlabs LED and collimating lens on the reader (Fig. 2) to provide a computer controlled bleaching unit with an irradiance of 0.6 W cm^{-2}. The impact of this UV LED on the IRPL

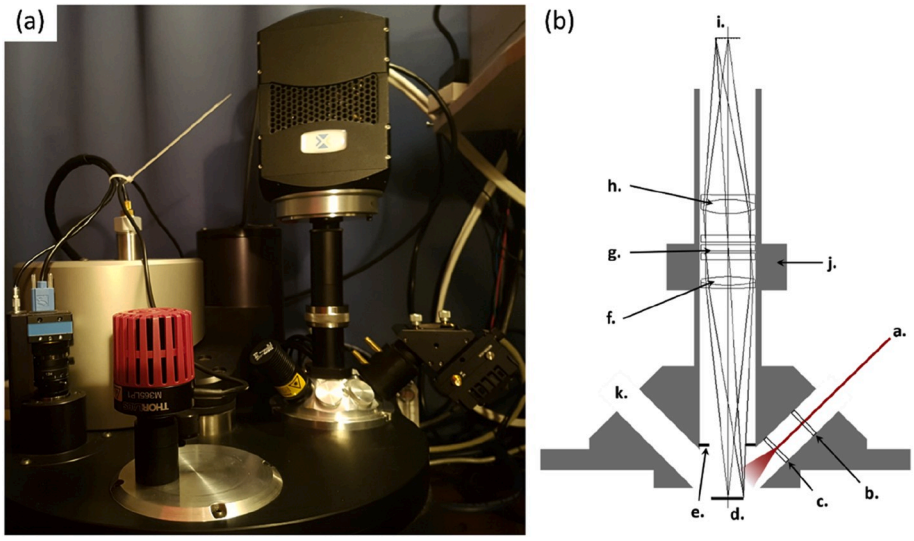

Fig. 2. Left: Photograph of the IRPL unit mounted on a Risø reader, with the EM-CCD mounted at the top. Also visible in the foreground (with the red housing) is the 365 nm LED used for bleaching the IRPL signal. Right: Schematic of the IRPL unit showing: (a) 850 nm stimulation laser; (b) laser clean-up filter (Edmund Optics™ 850 × 10nm); (c) ground glass diffuser; (d) the sample; (e) baffle; (f) 100 mm NIR achromatic doublet objective lens (Thorlabs™ AC254-100-B); (g) detection filters (Edmund Optics™ – two LP925 and one BP950 × 50nm); (h) 80 mm NIR achromatic doublet imaging lens (Thorlabs™ AC254-80-B); (i) Image plane – Photometrics™ EMCCD; (j) Focus mechanism; (k) Additional ports for LEDs, PMTs etc. Eight ports in total; (l) all internal surfaces painted matt black. (For interpretation of the references to colour in this figure legend, the reader is referred to the Web version of this article.)

and IRSL signal is discussed later in this paper.

The additional stimulation and bleaching units described above were connected to the External Light Source signals that are built into the DASH head (Lapp et al., 2015), and this allowed full automatic control of the new attachment with the standard software used for measuring sequences on Risø instruments.

2.1. Spatial discrimination of IRPL signal and breakthrough

Potassium-rich feldspar separated from an aeolian dune in North Island New Zealand (GDNZ16; Duller, 1996) was used for characterisation of this instrument. The sample had been sieved at 180–212 μm and undergone density separation at 2.62 and 2.58 g cm^{-3} to isolate a potassium-rich fraction. Grains of this material were mounted on single grain discs consisting of an array of 10 by 10 holes, each 300 μm deep and 300 μm in diameter. Optical stimulation at 850 nm was for 1.25 s, and an image was collected every 0.25 s or every 0.1 s (to aid comparison, values in the text are all expressed as counts per 0.1s). The IRPL image of the single grain disc shown in Fig. 3 was after a dose of ~100 Gy. Prior to this measurement the grains had been preheated at 260 °C for 60 s.

The single grain holder has a defined grid of 100 holes containing grains, and the three locating holes around the margins of the disc allow a coordinate system to be defined that marks where each grain hole is within the image (Duller et al., 1999; Kook et al., 2015). The defined geometry of the sample on the disc makes it possible to discriminate spatially between those regions where one would only expect to observe breakthrough, and those where one would expect to see IRPL (on top of any breakthrough). This spatial discrimination provides an alternative to the time resolved discrimination between signal and breakthrough described by Kook et al. (2018) for photomultipliers.

To measure breakthrough of the 850 nm stimulation into the detector and subtract it from the IRPL signal, two sets of regions of interest were defined for the EMCCD images collected. The first set of regions of interest are centred on each of the holes where the 100 grains are mounted (shown in red in Fig. 4(a)). The second set of regions of interest are centred between the grain holes in an 11 by 11 grid (shown in green in Fig. 4(a)). Thus each grain hole has 4 regions of interest around it where there should be no IRPL, and the average of these four values can be used to define the background due to breakthrough for that hole.

3. Initial characterisation of the instrument

Two sets of measurements were made, one using the Electron Multiplying mode of the EMCCD and one in non-EM mode. In non-EM mode the maximum intensity of the observed signal is ~4000 counts per pixel. Kook et al. (2015) recommended defining a region of interest 450 μm in diameter over each single grain hole in order to optimise the signal from each grain while minimising cross-talk from grains in adjacent holes. Summing the signal from this 0.16 mm^2 area, the intensity is up to 240,000 counts per 0.25 s, but this includes breakthrough from the 850 nm stimulation. Averaging the signal from regions of

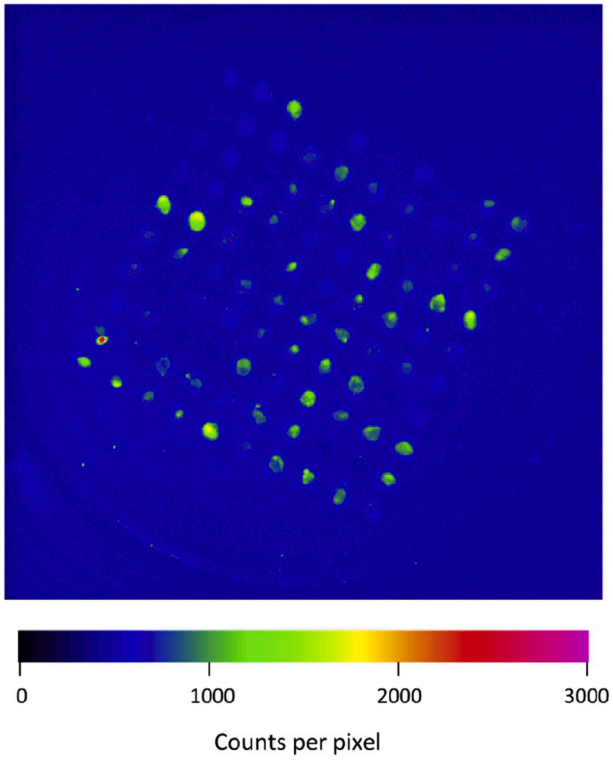

Fig. 3. Image of IRPL emission from a single grain disc with grains of potassium-rich feldspar from GDZN16. The image is 512 by 512 pixels and the field of view is approximately 10 mm across. This frame of the image was collected for a period of 0.1 s. The different colours in the image show the intensity of the IRPL signal per pixel. (For interpretation of the references to colour in this figure legend, the reader is referred to the Web version of this article.)

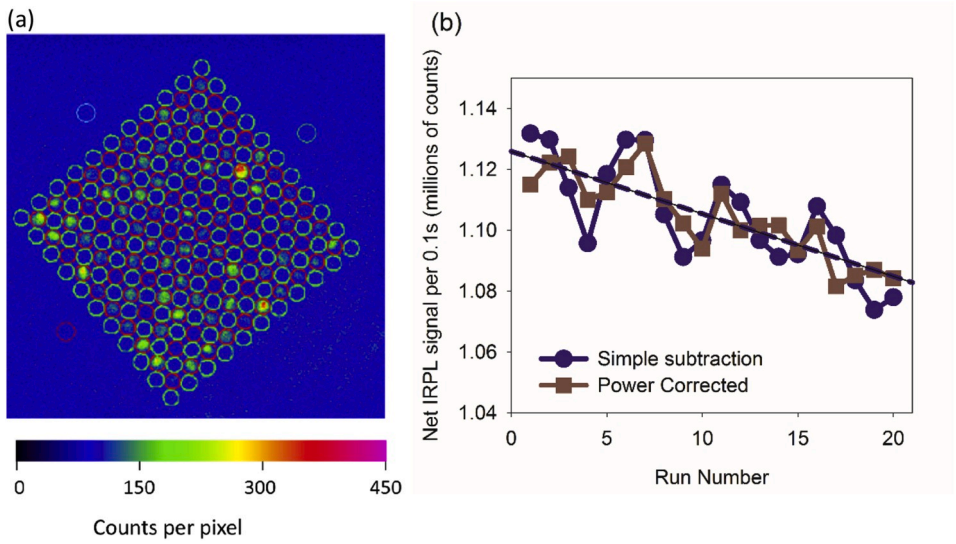

Fig. 4. (a) Regions of interest defined both to estimate the IRPL signal (shown as red circles) and to define the background due to breakthrough (shown as green circles). (b) Net IRPL signal for the holes with sample (red circles in part a). Each run involved 2.5 s of stimulation at 850 nm, but data are expressed as signal per 0.1s. (For interpretation of the references to colour in this figure legend, the reader is referred to the Web version of this article.)

interest (each 0.16 mm^2 in area) located away from the single grain holes gives a mean signal of 125657 ± 5441 counts or 279 ± 12 counts per pixel per 0.25s. In non-EM mode, CCD readout noise (noise introduced during the process of measuring the charge accumulated in each pixel) is significant, and is 11.1 counts per pixel. The remainder (~268 counts per pixel per 0.25s) of this signal arises from breakthrough of the 850 nm stimulation wavelength through the detection filters. In electron multiplying mode the dynamic range of the EMCCD is diminished, but the read noise is negligible. Analysis of the same sample in EM-mode gave a read noise of 0.003 counts per pixel and a signal of 228 ± 11 counts per pixel per 0.25s (equivalent to 91 counts per pixel per 0.1s).

To assess the reproducibility of the IRPL measurements, and to see whether the signal is depleted with repeated measurement, the sequence shown in Table 1 was used. In this analysis the signals from all 100 regions of interest centred on the grains have been summed, and the signal from the 121 ROIs used for the background scaled by a factor of 1.21 before subtracting it from the 100 ROIs where grains are located. The signal from breakthrough is ~100 counts per pixel per 0.1s, similar to the value of 91 counts per pixel per 0.1s obtained previously. After subtracting this background, the net signal averaged across all 100 grain holes is ~30 counts per pixel, equating to a total signal of ~1.1 million counts per 0.1s (Fig. 4(b)). A small decline in IRPL intensity is observed (0.18% per 2.5 s measurement), consistent with previous reports (Prasad et al., 2017). There is variability of 0.97% in the IRPL signal about a linear fit to the data (Fig. 4(b)), and it is likely that this results from variations in the power output from the 850 nm laser diode.

The intensity of IRPL measurements will depend linearly upon the power of the IR stimulation source, so having a stable power output from the 850 nm laser diode is important. The breakthrough of the 850 nm laser into the EMCCD detector as measured by the ROIs in between the 100 sample holes provides a direct measure of the intensity of the 850 nm stimulation, and so variations in this breakthrough from one measurement to another might be used to correct for minor variations in stimulation power.

To assess whether this method could correct for variations in stimulation power, the average breakthrough (as measured in the array of 121 ROIs shown as green circles in Fig. 4(a)) was divided by the average breakthrough measured over all 20 measurements, to calculate the relative power for each measurement cycle. This value of relative power was then used to normalise the net IRPL signal and calculate the power-corrected values shown in Fig. 4(b). This power-corrected data set shows the same trend as the uncorrected data, implying that for this data set there is no evidence for systematic changes in IR power. The power-corrected data shows slightly lower variability than the data after simple subtraction (0.62% compared with 0.97%), but the pattern of variability is the same as the original, implying that the correction has not been entirely successful. Since the uncorrected data showed very limited variability (0.97%), subsequent analysis has not used this form of power correction.

Table 1
Experimental procedure to assess the reproducibility of IRPL measurements and depletion of the signal with measurement time.

Step	
1	ß irradiation 665 Gy
2	TL to 260 °C at 5 °C.s^{-1} and hold for 60s
3	IR (880 nm) at 50 °C for 200s
4	IRPL (850 nm) at 50 °C for 2.5s (5s measurement time, including time before and after IR stimulation with no optical stimulation)
5	Repeat step 4 a total of 20 times

4. Impact of 365 nm illumination upon IRPL, IRSL and post-IR IRSL signals

To undertake a single aliquot regenerative dose (SAR) protocol, the luminescence signal needs to be reset after each measurement. The IRPL signal does not decrease rapidly with measurement time, so some other method of resetting the signal is needed. Prasad et al. (2017) used stimulation at 470 nm while holding the sample at 300 °C, but this was not possible using the instrument described here. Instead, a 1W 365 nm LED has been mounted on the reader. The sequence shown in Table 2(a) was used to measure the impact of exposure to this UV LED upon the IRPL signal. Since measurement causes negligible depletion of the IRPL signal, a single beta dose was given and preheated, prior to an alternating sequence of IRPL measurement and UV exposure, eventually giving a cumulative length of UV exposure of 20,000 s (Fig. 5). The same sample was then measured using the sequence in Table 2(b) to measure the impact of the UV exposure upon the IRSL and post-IR $IRSL_{225}$ signals and provide a point of comparison with previously published bleaching data for these signals (e.g. Colarossi et al., 2015; Buylaert et al., 2012). For these measurements a DASH head equipped with 870Δ45 nm LEDs was used along with the EMCCD and BG3 and BG39 filters to observe the

Table 2(a)
Impact of UV LED on the IRPL signal.

Step	
1	ß irradiation 665 Gy
2	TL to 260 °C at 5 °C.s^{-1} and hold for 60s
3	IR (880 nm) at 50 °C for 200s
4	IRPL (850 nm) at 50 °C for 2.5s (5s including off time before and after IR stimulation)
5	UV exposure for 0, 0, 2, 3, 5, 10, 30 etc seconds
6	Repeat steps 4 and 5 to a total cumulative UV exposure time of 20,000 s

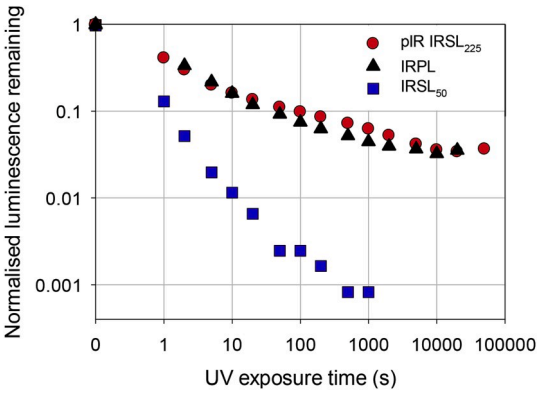

Fig. 5. Impact of 1W 365 nm UV LED upon different luminescence signals from feldspar. The procedure described in Table 2(a) was used for measurements of the IRPL signal and Table 2(b) for the $IRSL_{50}$ and pIR $IRSL_{225}$ signal.

~400 nm IRSL emission. As has been observed many times previously, the $IRSL_{50}$ signal is reset more rapidly than the post-IR $IRSL_{225}$ signal (Fig. 5). In spite of the slower rate of bleaching for the post-IR $IRSL_{225}$ signal it does appear to be well reset in many natural depositional environments and has proved to be a very valuable chronometer for dating sediments. The IRPL signal appears to bleach at a very similar rate as the post-IR $IRSL_{225}$ signal, and thus there is also potential for the IRPL signal in sediment dating applications. The solar spectrum in nature is very different to that from the 365 nm LED, and hence measurement of samples bleached in nature will be important in future work. The ability to look at grain to grain variations in the degree of resetting is clearly advantageous. This is explored in section 6, but before that, the temperature dependence of the IRPL and IRSL signals are compared.

5. Temperature dependence of IRPL and IRSL signals

The temperature dependence of the IRPL signal was investigated in order to decide the optimum temperature at which to make IRPL measurements using the attachment described here. Kumar et al. (2018) demonstrated that over the temperature range from 7 K to 295 K, the 955 nm IRPL emission remains constant from 7 K to ~200 K, and then drops from 200 K to 295 K, but does not reach zero. An aliquot of potassium rich feldspar from GDNZ16 was used to extend the temperature range for such measurements. The aliquot was given a beta dose of 166 Gy, preheated at 320 °C for 60 s and then had the IRSL signal measured using the 880 nm LED while holding the sample at 50 °C. Following this, the IRPL signal was measured at temperatures from 50 to 300 °C (323–573 K). After each measurement, the aliquot was bleached using the UV LED for 1200 s to remove the IRPL signal, and the aliquot was then irradiated again and the cycle repeated. The IRPL signal measured in the range 50–300 °C drops monotonically (Fig. 6), continuing the trend seen by Kumar et al. (2018) at lower temperatures. This drop has previously been interpreted as thermal quenching of the IRPL emission process (Kumar et al., 2018), and is in stark contrast to the increase in the IRSL signal that has been reported many times, as first seen by Duller and Wintle (1991).

Table 2(b)
Impact of UV LED on the IRSL and pIR $IRSL_{225}$ signal.

Step		Signal
1	ß dose 62 Gy	
2	TL to 260 °C at 5 °C.s^{-1} and hold for 60s	
3	UV exposure for 0, 1, 2, 5, 10, 20..50ks	
4	IRSL at 50 °C for 200s	$IRSL_{50}$
5	IRSL at 225 °C for 100s	pIR $IRSL_{225}$
6	UV exposure for 600s	
7	ß dose 52 Gy	
8	TL to 260 °C at 5 °C.s^{-1} and hold for 60s	
9	IRSL at 50 °C for 200s	$IRSL_{50}$
10	IRSL at 225 °C for 100s	pIR $IRSL_{225}$
11	UV exposure for 600s Repeat steps 1 to 11	

A similar experiment as described above was undertaken on the same sample, to provide direct comparison of the behaviour of the IRSL signal at different measurement temperatures. The procedure followed is identical to that used for the IRPL measurement except that following the preheat to 320 °C the IRSL signal is measured at the different temperatures for 200 s in order to deplete the IRSL signal. The IRSL signal increases in intensity by a factor of over 30 times in this temperature range. This increase is due to greater efficiency with which charge is excited from the ground state and subsequently transported via band-tail states to recombination centres (Jain and Ankjaergaard, 2011).

6. Single aliquot regenerative dose measurements

6.1. Measurement of a laboratory radiation dose

A single aliquot regenerative dose (SAR) protocol using the IRPL signal is shown in Table 3. Grains were exposed to the UV LED for 600 s after measurement of L_x and T_x in order to reduce the IRPL signal. To assess the effectiveness of the procedure the set of grains that had previously been measured to assess the impact of UV exposure upon the IRPL and IRSL signals were used. Grains were given a beta dose of 104 Gy, and then the sequence in Table 3 was followed to build up a dose response curve. The aim of this experiment was to see whether this SAR sequence was able to recycle a dose, and reset the IRPL signal. Fig. 7(a) shows the IRPL signal from a single grain in response to regeneration doses ranging from zero to 166 Gy. The background subtracted from this signal varies depending upon the signal measured in the four adjacent background ROIs, but is typically ~40,000 counts per 0.1s channel per ROI. The IRPL signal does not decline during the 2 s of stimulation at

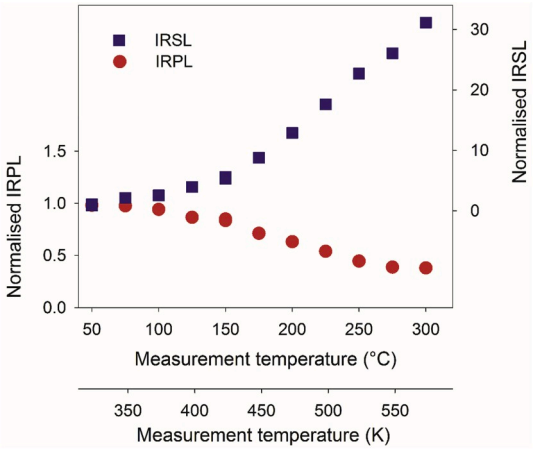

Fig. 6. Change in IRPL and IRSL signals with measurement temperature. Note the different y-axes used for the IRPL and IRSL data. The temperature is shown both in centigrade and kelvin to allow comparison with previously published data.

Table 3
Single aliquot regenerative dose (SAR) sequence used for IRPL measurements.

Step		Signal
1	Natural or Laboratory Irradiation	
2	Preheat to 260 °C at 5 °C.s^{-1} and then hold for 60s	
3	IR (880 nm) for 200s, sample at 50 °C	
4	IRPL (850 nm) for 2.5s (0.25s/image) at room temp	L_x
5	UV (365 nm) for 600 s at room temp	
6	Test Dose (52 Gy)	
7	Preheat to 260 °C at 5 °C.s^{-1} and then hold for 60s	
8	IR (880 nm) for 200s, sample at 50 °C	
9	IRPL (850 nm) for 2.5s (0.25s/image) at room temp	T_x
10	UV (365 nm) for 600 s at room temp	
11	Return to step 1	

850 nm (as expected from Fig. 4(b)) and the small variation in IRPL intensity during each measurement is thought to relate to fluctuations in the intensity of the 850 nm laser diode (cf. Fig. 4(b)). To reduce the impact of these small fluctuations, the IRPL signal is summed for the period from 2 to 4s. The signals obtained are then used to construct a dose response curve for each grain (e.g. Fig. 7(b)). Signals have been screened to accept only those grains where recycling is within 10% of unity, the uncertainty on the test dose is less than 10%, and signals grow monotonically. Of the 100 grains on the sample disc, 23 gave data suitable for constructing a dose response curve, and a radial plot of the D_e values is shown in Fig. 7(c). As would be expected where the grains have previously been conditioned in prior experiments, the D_e values do not show any overdispersion. The mean D_e value is 96.4 ± 1.5 Gy, 93% of the given dose of 104 Gy. The results demonstrate that the instrument is able to generate dose response curves from individual grains of feldspar, and that the SAR procedure in Table 3 is able to recover a given laboratory radiation dose.

6.2. Measurement of a natural radiation dose

A set of grains from GDNZ16 that had not previously been measured were placed in a single grain holder, and the sequence shown in Table 3 used to measure the natural IRPL signal and D_e from the grains. Of the 100 grains measured, 22 gave data that passed the rejection criteria outlined above. The IRPL dose response curve was measured to a maximum regenerative dose of 1325 Gy (e.g. Fig. 8(a)) and dose response curves have an average D_0 value of 261 Gy, but this value varied from 122 to 432 for individual grains. For the 22 grains for which a D_e value was obtained, the average background was 59291 ± 1717 counts per 0.25s (sum of ~450 pixels), and the average natural signal (including the background) from the 22 grains was 94201 ± 59291 counts per 0.25 s. Thus the average signal-to-noise ratio is only 0.59. In spite of this low signal-to-noise ratio, dose response curves such as that shown in Fig. 8(a) could be produced, and the radial plot shows that consistent D_e values were obtained (Fig. 8(b)). The overdispersion of the 22 IRPL D_e values is 22%, near the lower end of the range observed in the few examples of single grain IRSL data sets from potassium rich feldspars (e.g. Reimann et al., 2012; Neudorf et al., 2012; Smedley et al., 2016; Riedesel et al., 2018). The weighted mean IRPL D_e value obtained is 103 ± 5.8 Gy, 18% larger than the value of 87.0 ± 3.7 Gy obtained by Duller (1996). However, this earlier value may not be reliable since it used a single aliquot additive dose method that is no longer used, and it measured the IRSL emission at 50 °C but did not make any assessment of anomalous fading. To provide a more appropriate comparison, the D_e value for this sample was measured using a SAR protocol with a post-IR IRSL signal.

The IRPL head was replaced with the DASH head to allow IRSL measurements to be made. A second set of single grains of feldspar from GDNZ16 were mounted on single grain discs and a post-IR $IRSL_{225}$ SAR sequence applied. The SAR sequence is almost identical to that described in Table 3 except that the IRSL measurements were for 100 s while the sample was held at a temperature of 50 °C, and the IRPL measurement was replaced by a post-IR IRSL measurement for 200 s while holding the sample at 225 °C. For the post-IR $IRSL_{225}$ signal, a total of 76 grains of the 100 grains measured passed the rejection criteria and gave a weighted mean D_e of 105 ± 3.8 Gy (Fig. 8), indistinguishable from the IRPL value. The overdispersion of the post-IR $IRSL_{225}$ D_e data is 25%, similar to the IRPL value.

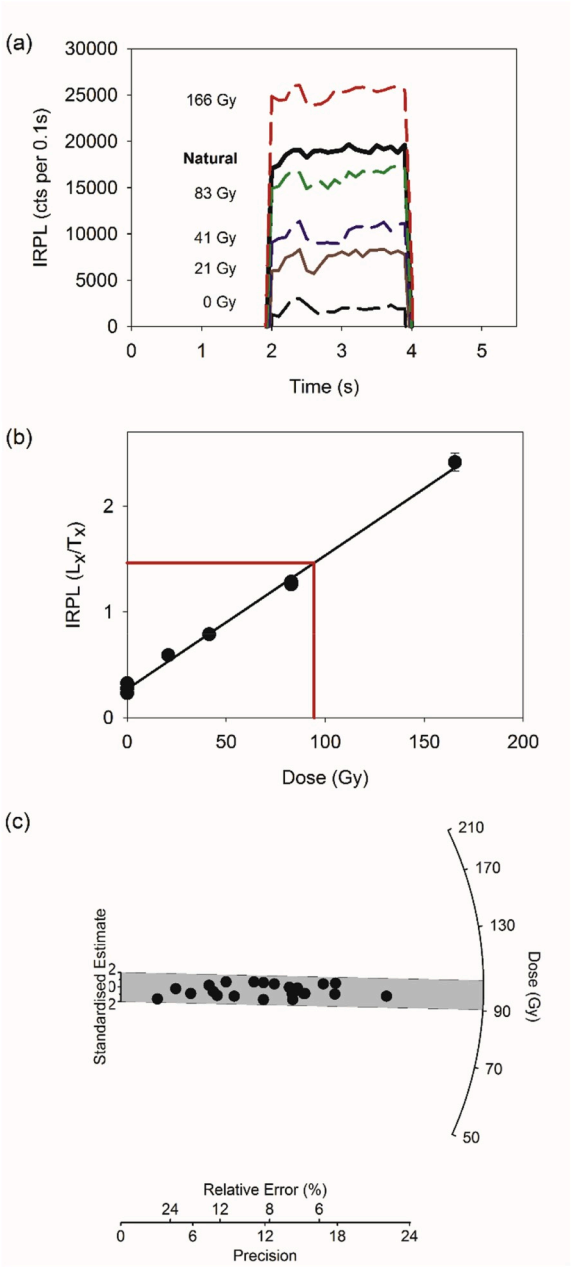

Fig. 7. IRPL instrument reproducibility assessment using single grains of GDNZ16. The grains were given a beta dose of 104 Gy before starting the SAR sequence. (a) An example of the net IRPL signal measured for a single grain after different regeneration doses varying from zero to 166 Gy. (b) The SAR dose response curve for the grain whose data are shown in (a). (c) Radial plot of D_e values obtained for 23 grains. The overdispersion is zero demonstrating the reproducibility of the attachment, and the recovered dose is 96.4 ± 1.5 Gy, 93% of the given dose of 104 Gy.

7. Conclusions

The use of an optical system designed to maximise the effectiveness

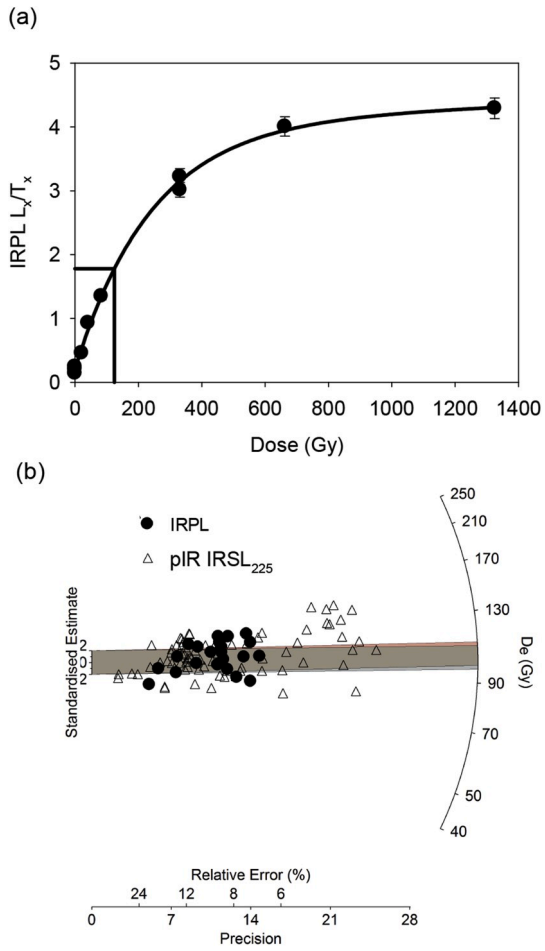

Fig. 8. (a) IRPL dose response curve for a single grain of GDNZ16. (b) Radial plot of D_e values for grains of GDNZ16. D_e data are shown from IRPL measurements (filled circles) and from post-IR $IRSL_{225}$ measurements (open triangles).

of the LP925 and BP950 rejection filters, and using the well-defined spatial definition of the sample within the image has made possible an IRPL system for single grains based on an EM-CCD detector. Although the signal-to-noise ratio is still low in comparison with the performance typically achieved for IRSL measurements, this IRPL system is able to generate reproducible data, with a typical variability of less than 1% between replicate measurements of the same sample (Fig. 4(b)). The 955 nm IRPL emission is strongly affected by thermal quenching, with the signal dropping monotonically from 50 °C to 300 °C (Fig. 6), and thus subsequent measurements of IRPL have been made at room temperature to maximise the signal. A single aliquot regenerative dose (SAR) method has been applied, using a UV LED to reset the IRPL signal between regeneration cycles. A dose recovery experiment demonstrates the reproducibility of the IRPL measurements, that a dose can be recovered within 10% of the given dose, and the suitability of the UV LED for resetting the signal. The natural D_e for single grains of an aeolian dune sand (GDNZ16) from New Zealand measured using IRPL (103 ± 5.8 Gy) is consistent with the value derived using a post-IR $IRSL_{225}$ signal (105 ± 3.8 Gy). The age control for GDNZ16 is poorly constrained (Duller, 1996) so it is not possible to assess the accuracy of this D_e determination, but future work using IRPL will focus on analysis of samples with robust independent age control in order to assess the accuracy of ages that can be calculated using this new signal.

Whilst the breakthrough from the 850 nm stimulation is high, one of the advantages of working with an imaging detector and a sample that is clearly defined within the field of view is that the background can be measured by analysis of areas away from the sample and subtracted. Reducing the breakthrough from the 850 nm stimulation will be important in future developments, but subtraction of the background in this way provides a system capable of measuring the IRPL signal from single grains suitable for dating.

Declaration of competing interest

The authors declare that they have no known competing financial interests or personal relationships that could have appeared to influence the work reported in this paper.

Acknowledgements

This work was supported by the UK Space Agency CREST3 program under grant ST/P001998/1. Research in Next Generation Luminescence methods in Aberystwyth is supported by NERC grant CC003, and by HEFCW infrastructure funding for SPARCL. Colleagues at DTU NuTech (especially MyungHo Kook and Per Sørensen) are gratefully thanked for their advice about interfacing to the DA-20 TL/OSL instrument. The two anonymous referees are thanked for their comments which helped to improve the clarity of the manuscript.

References

Buylaert, J.-P., Jain, M., Murray, A.S., Thomsen, K.J., Thiel, C., Sohbati, R., 2012. A robust feldspar luminescence dating method for Middle and Late Pleistocene sediments. Boreas 41, 435–451.
Colarossi, D., Duller, G.A.T., Roberts, H.M., Tooth, S., Lyons, R., 2015. Comparison of paired quartz OSL and feldspar post-IR IRSL dose distributions in poorly bleached fluvial sediments from South Africa. Quat. Geochronol. 30, 233–238.
Duller, G.A.T., 1996. The age of the Koputaroa dunes, southwest North Island, New Zealand. Palaeogeogr. Palaeoclimatol. Palaeoecol. 121, 105–114.
Duller, G.A.T., 2008. Single grain optical dating of Quaternary sediments: why aliquot size matters in luminescence dating. Boreas 37, 589–612.
Duller, G.A.T., Bøtter-Jensen, L., Kohsiek, P., Murray, A.S., 1999. A high-sensitivity optically stimulated luminescence scanning system for measurement of single sand-sized grains. Radiat. Protect. Dosim. 84, 325–330.
Duller, G.A.T., Bøtter-Jensen, L., Murray, A.S., 2003. Combining infrared- and green-laser stimulation sources in single-grain luminescence measurements of feldspar and quartz. Radiat. Meas. 37, 543–550.
Duller, G.A.T., Kook, M., Stirling, R.J., Roberts, H.M., Murray, A.S., 2015. Spatially-resolved thermoluminescence from snail opercula using an EMCCD. Radiat. Meas. 81, 157–162.
Duller, G.A.T., Wintle, A.G., 1991. On infrared stimulated luminescence at elevated temperatures. Nucl. Tracks Radiat. Meas. 18, 379–384.
Jain, M., Ankjaergaard, C., 2011. Towards a non-fading signal in feldspar: insight into charge transport and tunnelling from time-resolved optically stimulated luminescence. Radiat. Meas. 46, 292–309.
Kook, M., Lapp, T., Murray, A.S., Thomsen, K.J., Jain, M., 2015. A luminescence imaging system for the routine measurement of single-grain OSL dose distributions. Radiat. Meas. 81, 171–177.
Kook, M., Kumar, R., Murray, A.S., Thomsen, K.J., Jain, M., 2018. Instrumentation for the non-destructive optical measurement of trapped electrons in feldspar. Radiat. Meas. 120, 247–252.
Kumar, R., Kook, M., Murray, A.S., Jain, M., 2018. Towards direct measurement of electrons in metastable states in K-feldspar: do infrared-photoluminescence and radioluminescence probe the same trap? Radiat. Meas. 120, 7–13.
Lapp, T., Kook, M., Murray, A.S., Thomsen, K.J., Buylaert, J.P., Jain, M., 2015. A new luminescence detection and stimulation head for the Risø TL/OSL reader. Radiat. Meas. 81, 178–184.
Neudorf, C.M., Roberts, R.G., Jacobs, Z., 2012. Sources of overdispersion in a K-rich feldspar sample from north-central India: insights from De, K content and IRSL age distributions for individual grains. Radiat. Meas. 47, 696–702.
Prasad, A.K., Poolton, N.R.J., Kook, M., Jain, M., 2017. Optical dating in a new light: a direct, non-destructive probe of trapped electrons. Sci. Rep. 7, 12097.
Reimann, T., Thomsen, K.J., Jain, M., Murray, A.S., Frechen, M., 2012. Single-grain dating of young sediments using the pIRIR signal from feldspar. Quat. Geochronol. 11, 28–41.
Riedesel, S., Brill, D., Roberts, H.M., Duller, G.A.T., Garrett, E., Zander, A.M., King, G.E., Tamura, T., Burow, C., Cunningham, A., Seeliger, M., DeBatist, M., Heyvaert, V.M. A., Fujiwara, O., Brückner, H., 2018. Single-grain feldspar luminescence chronology

of historical extreme wave event deposits recorded in a coastal lowland, Pacific coast of central Japan. Quat. Geochronol. 45, 37–49.
Smedley, R.K., Glasser, N.F., Duller, G.A.T., 2016. Luminescence dating of glacial advances at lago Buenos Aires (~46 °S), Patagonia. Quat. Sci. Rev. 134, 59–73.
Thomsen, K.J., Kook, M., Murray, A.S., Jain, M., Lapp, T., 2015. Single-grain results from an EMCCD-based imaging system. Radiat. Meas. 81, 185–191.